Tight-binding model for graphene

Michael Sullivan
8615173

PHYS 40182
Final MPhys project report

Supervised by:
Dr. Yang Xian

School of Physics and Astronomy
The University of Manchester

May 2017

Abstract

The world's first two-dimensional material, known as graphene, has captured the attention of scientists and researchers worldwide due to its many useful and surprising properties such as its controllable optical transparency, immense strength and high mobility at room temperature [1]. Widespread applications have already been discovered for the novel material such as membrane technology, energy storage, sensors and nanoelectronics, with many more to be found in the future. In recent years, research has developed in the concept of using graphene in nanodevices for applications in computation memory and storage, however this requires the use of geometries small enough that considering a graphene sheet as infinite is no longer valid. By considering finite width graphene systems, which are called nanoribbons, it will be found that new properties emerge as a direct consequence of the fact the geometry is finite, namely the existence of "edge states". These edge states are of great interest as they have the potential to be used in spintronic applications due to the presence of spin-dependant currents [2]. As well as this, graphene nanoribbons can be chosen to be either an electronically conducting or insulating material depending on the width of the ribbon itself, however this does introduce issues with producing a sample of graphene with specific properties in the laboratory, but this will not be discussed here. If finite graphene ribbons are to be used in nano-electronic devices, it also becomes apparent that the behaviour of graphene needs to be understood at both in finite-sized system but also in the presence of a general magnetic field, for which there are many papers in the literature [3,4,5]. In this report, the electronic properties of both infinite and finite graphene systems will be investigated by use of the tight-binding model of the electrons on a two-dimensional honeycomb lattice. This will be used to derive the energy band structures for both infinite and finite systems by diagonalising the relevant Hamiltonian via both analytical methods and numerical analysis where applicable. These methods will then be extended to developing the theory for both systems of graphene when in the presence of a magnetic field, where the behaviour of the edge states will be further explored.

1. Electronic properties of the graphene sheet

Monolayer graphene has a hexagonal or honeycomb structure of carbon atoms, each carbon atom with three neighbours, joined by sigma covalent bonds. The electronic configuration of carbon is $1s^2 2s^2 2p^2$, however the energy difference between the $2s$ and $2p$ orbitals allows for a mixed states of these orbitals to exist. In this state, it becomes energetically favourable to excite an electron from the $2s$ orbital to the $2p$ orbital. The $2p$ orbital can be broken down into $2p_x, 2p_y$ and $2p_z$ orbitals, each containing an electron, with the *x-y* orbitals in the plane of the lattice and the *z* orbital perpendicular. The mixed *x-y orbitals* form the sigma bonds with the three nearest neighbours, with the remaining electron in the *z* orbital forming pi bond with nearest neighbours, i.e. a side on overlap of the electron wavefunctions. These pi electrons determine the energy bands of graphene and will be studied using the tight binding model.

Considering an independent atom, the wavefunction of the atomic orbitals $\varphi^{(a)}(\mathbf{r})$ are eigenvalues of the atomic Hamiltonian, however in a crystal, these wavefunctions overlap and are no longer true eigenvalues of the atomic Hamiltonian. This situation is well studied and the solution is known as Bloch's Theorem or the Bloch wavefunction:

$$\psi_{\mathbf{k}}(\mathbf{r}) = \sum_{\mathbf{R}_j} \exp(i\mathbf{k}\cdot\mathbf{R}_j)\varphi^{(a)}(\mathbf{r}-\mathbf{R}_j), \tag{1}$$

where $\mathbf{R}_j = m_j\mathbf{a}_1 + n_j\mathbf{a}_2$ are the Bravis lattice vectors of the lattice. In graphene, a unit cell contributes two atoms so this wavefunction must be modified. Also, graphene can be considered to consist of two intertwining sublattice that we label A and B, as illustrated in figure 1.

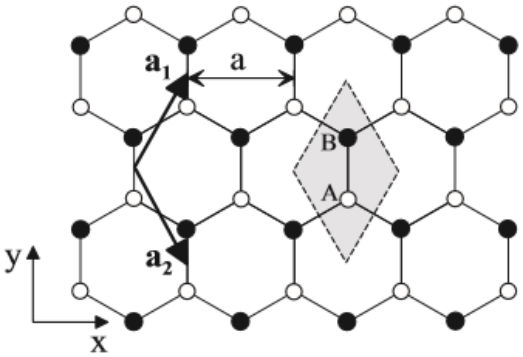

Figure 1. A diagram illustrating the hexagonal structure of a monolayer graphene lattice, with two sublattices A and B. A unit cell is shown in the shaded region. [1]

A translation of any vector that connects a site on the A sublattice to one of the B sublattice is not a symmetry translation as only one of them is a lattice point. This can also be said by noting that a translation operation which carries this out does not commute with the Hamiltonian. As there is a lack of symmetry between the two sublattices, they must be considered separately and described by different wavefunctions. The trial wavefunction of the two electrons is:

$$\psi_{\mathbf{k}}(\mathbf{r}) = a_{\mathbf{k}}\,\psi_{\mathbf{k}}^{(A)}(\mathbf{r}) + b_{\mathbf{k}}\,\psi_{\mathbf{k}}^{(B)}(\mathbf{r}), \tag{2}$$

where $a_{\mathbf{k}}$ and $b_{\mathbf{k}}$ are complex functions which are dependent on the quasi-momentum $\mathbf{k}$. The time independent Schrödinger equation $\hat{H}\psi_{\mathbf{k}}(\mathbf{r}) = \varepsilon_{\mathbf{k}}\psi_{\mathbf{k}}(\mathbf{r})$ gives after multiplying by $\psi_{\mathbf{k}}^{*}(\mathbf{r})$:

$$\begin{pmatrix} a_{\mathbf{k}}^{*} & b_{\mathbf{k}}^{*} \end{pmatrix} \begin{pmatrix} \psi_{\mathbf{k}}^{(A)*}\hat{H}\psi_{\mathbf{k}}^{(A)} & \psi_{\mathbf{k}}^{(A)*}\hat{H}\psi_{\mathbf{k}}^{(B)} \\ \psi_{\mathbf{k}}^{(B)*}\hat{H}\psi_{\mathbf{k}}^{(A)} & \psi_{\mathbf{k}}^{(B)*}\hat{H}\psi_{\mathbf{k}}^{(B)} \end{pmatrix} \begin{pmatrix} a_{\mathbf{k}} \\ b_{\mathbf{k}} \end{pmatrix} = \begin{pmatrix} a_{\mathbf{k}}^{*} & b_{\mathbf{k}}^{*} \end{pmatrix} \begin{pmatrix} \psi_{\mathbf{k}}^{(A)*}\psi_{\mathbf{k}}^{(A)} & \psi_{\mathbf{k}}^{(A)*}\psi_{\mathbf{k}}^{(B)} \\ \psi_{\mathbf{k}}^{(B)*}\psi_{\mathbf{k}}^{(A)} & \psi_{\mathbf{k}}^{(B)*}\psi_{\mathbf{k}}^{(B)} \end{pmatrix} \begin{pmatrix} a_{\mathbf{k}} \\ b_{\mathbf{k}} \end{pmatrix}, \tag{3}$$

$$\begin{pmatrix} a_{\mathbf{k}}^{*} & b_{\mathbf{k}}^{*} \end{pmatrix} \mathbf{H}_{\mathbf{k}} \begin{pmatrix} a_{\mathbf{k}} \\ b_{\mathbf{k}} \end{pmatrix} = \begin{pmatrix} a_{\mathbf{k}}^{*} & b_{\mathbf{k}}^{*} \end{pmatrix} \mathbf{S}_{\mathbf{k}} \begin{pmatrix} a_{\mathbf{k}} \\ b_{\mathbf{k}} \end{pmatrix}, \tag{4}$$

where the overlap matrix $\mathbf{S}_{\mathbf{k}}$ and the Hamiltonian $\mathbf{H}_{\mathbf{k}}$ are defined by the matrices in equation (3). The Schrödinger equation for this system has now been transformed into the form of an eigenvalue equation which has solution:

$$\left| \mathbf{H}_{\mathbf{k}} - \varepsilon_{\mathbf{k}}^{\lambda}\, \mathbf{S}_{\mathbf{k}} \right| = 0, \tag{5}$$

where λ denotes the energy bands of the pi electrons. For n atoms per unit cell, it can be written:

$$\psi_{\mathbf{k}} = \sum_{j=1}^{n} a_{\mathbf{k}}^{(j)} \psi_{\mathbf{k}}^{(j)}; \qquad \mathbf{H}_{\mathbf{k}}^{ij} \equiv \psi_{\mathbf{k}}^{(i)*} H \psi_{\mathbf{k}}^{(j)}; \qquad \mathbf{S}_{\mathbf{k}}^{ij} \equiv \psi_{\mathbf{k}}^{(i)*} \psi_{\mathbf{k}}^{(j)}, \tag{6}$$

and recalling $\psi_{\mathbf{k}}^{(j)}(\mathbf{r}) = \sum_{\mathbf{R}_l} \exp(i\mathbf{k}\cdot\mathbf{R}_l)\varphi^{(j)}(\mathbf{r} - \mathbf{R}_l + \delta_j)$, where we define δ_j to be a vector relating the sublattices A and B, we find that:

$$\mathbf{H}_{\mathbf{k}}^{ij} = N\left(\varepsilon^{(i)}\mathbf{s}_{\mathbf{k}}^{ij} + t_{\mathbf{k}}^{ij}\right), \tag{7}$$

$$\mathbf{s}_{\mathbf{k}}^{ij} = \sum_{\mathbf{R}_l} \exp(i\mathbf{k}\cdot\mathbf{R}_l) \int d^2 r\, \varphi^{(i)*}(\mathbf{r} + \delta_i - \mathbf{R}_l)\, \varphi^{(j)}(\mathbf{r} + \delta_j - \mathbf{R}_l) = \mathbf{S}_{\mathbf{k}}^{ij} / N, \tag{8}$$

$$t_{\mathbf{k}}^{ij} = \sum_{\mathbf{R}_l} \exp(i\mathbf{k}\cdot\mathbf{R}_l) \int d^2 r\, \varphi^{(i)*}(\mathbf{r} + \delta_i - \mathbf{R}_l) \Delta V\, \varphi^{(j)}(\mathbf{r} + \delta_j - \mathbf{R}_l), \tag{9}$$

where $\mathbf{s}_{\mathbf{k}}^{ij}$ is termed the overlap correction and $t_{\mathbf{k}}^{ij}$ is the hopping matrix. The potential ΔV arises from the interaction between the neighbouring atoms where the pi electron wavefunctions overlap. The eigenvalue equation now becomes:

$$\left| t_{\mathbf{k}}^{ij} - \varepsilon_{\mathbf{k}}^{\lambda}\, \mathbf{s}_{\mathbf{k}} \right| = 0, \tag{10}$$

where an overall shift in the energy levels has been neglected as all atomic orbitals considered are identical. It can be chosen that the Bravis lattice vectors that connect sublattice A and the equivalent site on the B sublattice is achieved by a displacement δ_3. The hopping amplitude between nearest neighbours and next nearest neighbours is then given by:

$$t \equiv \int d^2 r\, \varphi^{A^*}(\mathbf{r}) \Delta V\, \varphi^{B}(\mathbf{r}+\delta_3), \tag{11}$$

$$t_{nnn} \equiv \int d^2 r\, \varphi^{A^*}(\mathbf{r}) \Delta V\, \varphi^{A}(\mathbf{r}+\mathbf{a}_1) = \int d^2 r\, \varphi^{\mathbf{B}^*}(\mathbf{r}) \Delta V\, \varphi^{B}(\mathbf{r}+\mathbf{a}_1), \tag{12}$$

and the overlap correction is given by:

$$t \equiv \int d^2 r\, \varphi^{A^*}(\mathbf{r})\, \varphi^{B}(\mathbf{r}+\delta_3). \tag{13}$$

It can be seen from equation (9) that for an arbitrary site on sublattice A, there are three off-diagonal terms that correspond to the nearest neighbours denoted B_1, B_2 and B_3 which all have the same hopping amplitude. However, these sites are described by different lattice vectors $\mathbf{R}_l$ and hence pick up a phase factors that come from the summation in (9). These off-diagonal terms can be written as:

$$t_{\mathbf{k}}^{AB} = t\gamma_{\mathbf{k}}^{*} = \left(t_{\mathbf{k}}^{BA}\right)^{*}; \qquad s_{\mathbf{k}}^{AB} = s\gamma_{\mathbf{k}}^{*} = \left(s_{\mathbf{k}}^{BA}\right)^{*}, \tag{14}$$

where

$$\gamma_{\mathbf{k}} \equiv 1 + \exp(i\mathbf{k}\cdot\mathbf{a}_1) + \exp(i\mathbf{k}\cdot\mathbf{a}_3), \tag{15}$$

and the diagonal terms are given by the nnn contributions, which when considering the phase factors picked up can be expressed as:

$$t_{\mathbf{k}}^{AA} = 2t_{nnn}\sum_{i=1}^{3}\cos(\mathbf{k}\cdot\mathbf{a}_i) = t_{nnn}\left(|\gamma|^2 - 3\right). \tag{16}$$

Now using (10), substituting the relevant equations and solving for the energy eigenvalues, the dispersion relation is found to be:

$$\varepsilon_{\mathbf{k}}^{\lambda} = \frac{t^{AA} + \lambda t|\gamma_k|}{1 + s|\gamma_k|}, \tag{17}$$

where $\lambda = \pm 1$ correspond to the valence and conduction bands. While (17) is a simple expression, it can be further simplified by assuming that the overlap integral and the next nearest neighbour hopping terms are considerably smaller than the nearest neighbour hopping, which has been verified by experiment [6]. Using these assumptions and neglecting any constant terms, as these just arbitrarily shift the energy relation and do not contribute to the overall behaviour, the energy bands can be expressed in the more useful form:

$$\varepsilon_{\mathbf{k}}^{\lambda} = 2t'_{nnn}\sum_{i=1}^{3}\cos(\mathbf{k}\cdot\mathbf{a}_i) + \lambda t\sqrt{3 + 2\sum_{i=1}^{3}\cos(\mathbf{k}\cdot\mathbf{a}_i)}, \tag{18}$$

where $t'_{nnn} = (t_{nnn} - st)$ can be considered as the overlap correction yielding a renormalisation of the hopping amplitudes. The energy dispersion (18) is plotted in figure 2, for the hopping

amplitude ratio $t'_{nnn}/t = 0.1$. It can be seen from figure 2 that the valence and conduction bands touch at point where equations (18) is identically zero. As the conduction band is filled with electrons and the valence band is completely empty, the Fermi level is then located at these points where (18) equals zero. These points are named Dirac points, and it can be shown that while there are six Dirac points, there are only two of these that are independent and are designated $\mathbf{K}$ and $\mathbf{K}'$. By setting $\varepsilon_{\mathbf{k}}^{\lambda} = 0$ and solving for $\mathbf{k}$, it is found that the Dirac points are:

$$\mathbf{K} = \frac{2\pi}{a}\left(\frac{1}{3}, \frac{1}{\sqrt{3}}\right), \qquad \mathbf{K} = \frac{2\pi}{a}\left(\frac{2}{3}, 0\right), \tag{19}$$

where a is the lattice constant.

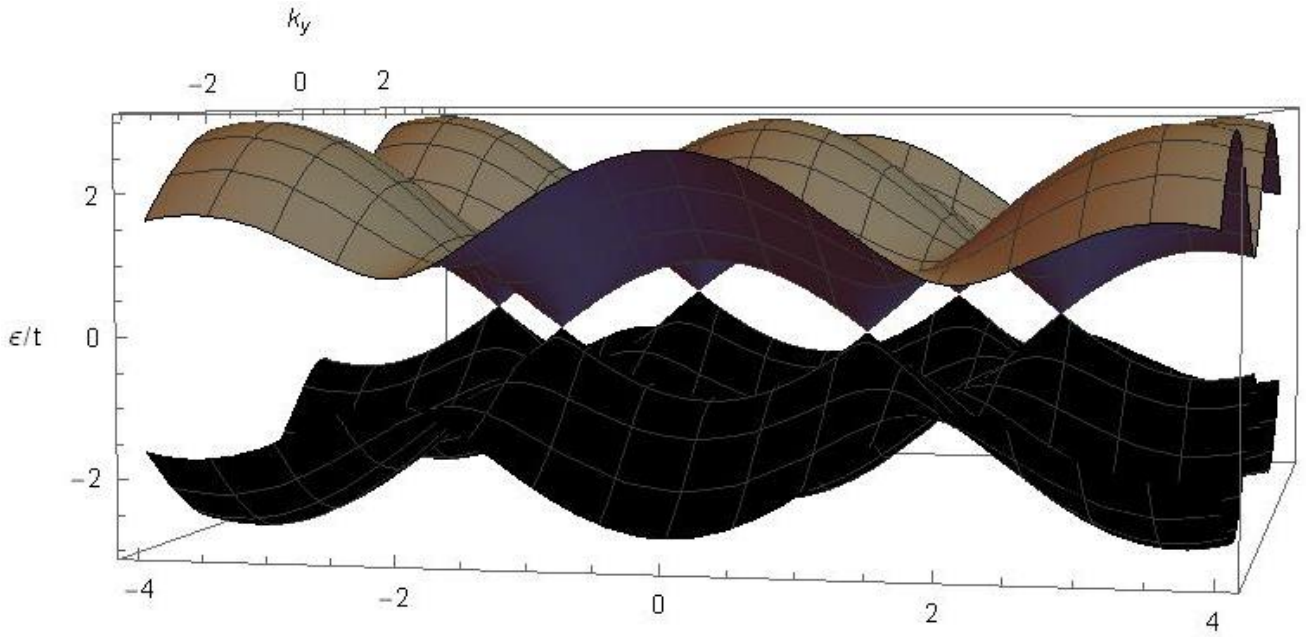

Figure 2. A plot of the dispersion relation of pi electrons in graphene (equation (18)). Here both valence and conduction bands are shown, which touch at the Dirac points in the k space. It should be noted that for small wavenumber (or long wavelength) excitations, the energy dispersion is linear and resembles that of a photon. For this reason, the electrons in graphene are often called massless Dirac electrons and are described by the Dirac equation [7]. Plotted in Wolfram Mathematica [8].

2. Armchair graphene nanoribbons

As the mobility and other electronic properties of graphene are desirable properties for electronic components, research in this area has led to understanding how graphene behaves when the lattice is not infinite. In the previous consideration of graphene, the lattice has been assumed to be infinite which the mathematics has reflected i.e. in the use of an infinite Fourier transform. While this method is very good at describing a large system, it fails at describing the finite system due to the emergence of edge states which have large implications on the low energy π electrons [6]. When the graphene lattice is cut in different directions, it is found that the geometry of the edges fall into three different categories: armchair, zigzag, or some combination of the two. Practically, when cutting graphene

nanoribbons from carbon nanotubes or growing the lattice, it is difficult to control which one of the edge orientations the sheet will have [9] , so it becomes a necessity to understand the behaviour and properties of both of the systems in order to realise nanoscale graphene electronic devices. In this paper, the nearest neighbour tight binding model will be applied to both the armchair and zigzag geometries, and analytical solutions to the energy eigenvalue problem will be found, hence giving the associated dispersion relations. In addition to this, a wave mechanics approach will be utilised, which allows the band structure to be found by quantising the transverse wavenumber subject to geometry dependant boundary conditions. This is where the differences between the two systems becomes apparent and explains the varied electronic properties along the edges of a graphene sheet produced in a laboratory [10].

A simple method used to describe the armchair nanoribbons is the one shown by figure 3, where the rows of carbon sites are labelled from 0 to N and describe the width of the nanoribbon.

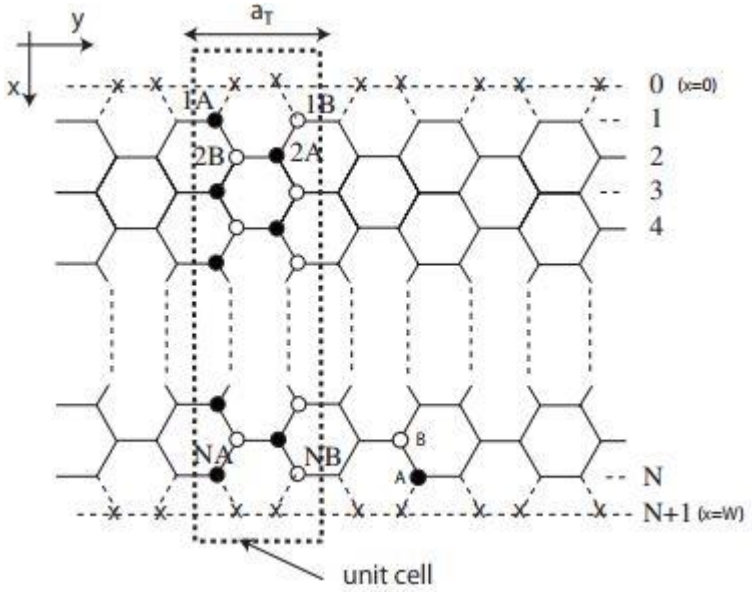

Figure 3. Diagram depicting the model used to describe armchair graphene nanoribbons, where the "x"s label places where the carbon lattice terminate with a hydrogen atom, which do not contribute to the electronic band structure. The A and B sublattices are distinguished by filled and open circles, and the dotted line labels the unit cell for this structure. Adapted from [11].

The unit cell width is denoted a_T and the sublattices are distinguished by the notation "XP" where X is the discretised position of the carbon atom in the x-direction and $P = A, B$ for the A and B sublattices respectively. With this notation, it becomes useful to describe the tight-binding Hamiltonian of the system in terms of fermionic creation and annihilation operators [11]:

$$\begin{aligned} H = &-t\sum_l \left\{ \sum_{m\,odd} a_l^\dagger(m) b_{l-1}(m) + \sum_{m\,even} a_l^\dagger(m+1) b_l(m) \right\} + h.c. \\ &-t\sum_l \sum_{m=1}^{N-1} \left\{ b_l^\dagger(m+1) a_l(m) + a_l^\dagger(m+1) b_l(m) \right\} + h.c. \end{aligned} \quad , \qquad (20)$$

where $a_l^\dagger(m)$ and $b_l^\dagger(m)$ create an electron at the mA and mB sites in the lth unit cell of the lattice respectively. Similarly $a_l(m)$ and $b_l(m)$ are the corresponding annihilation operators. The first line in (20) can be considered to describe the longitudinal hopping of an electron along the y-direction of the lattice, i.e. along the unit cells, whereas the second line describes the transverse electron hopping along the x-axis. As these operators describe electrons, which are fermions, they must obey the fermionic anticommutation relations:

$$\left\{a_l(m), a_{l'}^\dagger(m')\right\} = \left\{b_l(m), b_{l'}^\dagger(m')\right\} = \delta_{ll'}\,\delta_{mm'}, \tag{21}$$

and all other anticommutations are equal to zero. To transform the Hamiltonian into a more useful form, a Fourier transformation is applied along the translationally invariant y-axis:

$$a_l(m) = \frac{1}{\sqrt{L_y}}\sum_k \exp(iky_{l,mA})\alpha_k(m), \quad b_l(m) = \frac{1}{\sqrt{L_y}}\sum_k \exp(iky_{l,mB})\beta_k(m), \tag{22}$$

where $y_{l,mA}\left(y_{l,mB}\right)$ is defined to be the y-coordinate in the lth unit cell, at the mA (mB) site in the lattice, where the lattice has L_y unit cells. Due to the hexagonal structure of the lattice, there is a difference in phase between the sites y_{mA} and $y_{(m+1)B}$ which can be absorbed into the wavefunctions. This allows the y-coordinates to be redefined as $y_{l,1A} = y_{l,2B} = y_{l,3A} = \ldots \equiv y_l$ and $y_{l,1B} = y_{l,2A} = y_{l,3B} = \ldots \equiv y_l + a_T/2$. Combining these with the periodic boundary condition $a_{l+L_y}(m) = a_l(m)$, the wavenumber becomes discrete:

$$k = \frac{2\pi}{L_y}w, \qquad w = 0, \pm 1, \pm 2, \ldots, \pm\frac{L_y}{2} - 1, \frac{L_y}{2}. \tag{23}$$

It is worth noting that for the infinite graphene system where $L_y \to \infty$, that the wavenumber comes continuous which reassuringly matches the previous consideration of the infinite graphene sheet. For the armchair nanoribbon system, it is assumed that L_y has a finite value. Defining a one-particle state in this system, for electron creation in both the A and B sublattices:

$$\left|\Psi(k)\right\rangle = \sum_m \left(\psi_{m,A}\,\alpha_k^\dagger(m) + \psi_{m,B}\,\beta_k^\dagger(m)\right)\left|0\right\rangle, \tag{24}$$

where $\left|0\right\rangle$ is the vacuum Fock state of the system. Substituting this one-particle state with the Schrödinger equation yields the equations of motion of the system:

$$\left.\begin{aligned} E\psi_{m,A} &= -\exp(-ik/2)\psi_{m,B} - \psi_{m-1,B} - \psi_{m+1,B}, \\ E\psi_{m,B} &= -\exp(ik/2)\psi_{m,A} - \psi_{m-1,A} - \psi_{m+1,A}, \end{aligned}\right\} \qquad m = 1, 2, 3, \ldots, N. \tag{25}$$

where the wavenumber ranges from $-\pi \le k \le \pi$. These equations of motion do not consider the edge of the graphene sheet as the wavefunction of the $0A, 0B, (N+1)A$ and $(N+1)B$

sites are undefined. If it is assumed that the wavefunctions fall to zero as a boundary condition at these sites, then the equations of motion at the edge sites are:

$$\begin{aligned} E\psi_{1,A} &= -\exp(ik/2)\psi_{1,B} - \psi_{2,B}, & E\psi_{N,A} &= -\exp(ik/2)\psi_{N,B} - \psi_{N-1,B}, \\ E\psi_{1,B} &= -\exp(-ik/2)\psi_{1,A} - \psi_{2,A}, & E\psi_{N,B} &= -\exp(-ik/2)\psi_{N,A} - \psi_{N-1,A}. \end{aligned} \tag{26}$$

The equations (25) can be solved by assuming a general form of the wavefunctions $\psi_{m,A} = A\exp(ipm) + B\exp(-ipm)$ and $\psi_{m,B} = C\exp(ipm) + D\exp(-ipm)$ where A, B, C and D are constants and p is the wavenumber in the transverse direction. Substituting these forms into (25) yields the simple equation from which the energy can be found:

$$\begin{vmatrix} E & \varepsilon_p + \exp(-ik/2) \\ \varepsilon_p + \exp(ik/2) & E \end{vmatrix} = 0 \quad \Rightarrow E_s = s\sqrt{1 + 2\varepsilon_p \cos(k/2) + \varepsilon_p^2} \tag{27}$$

where $\varepsilon_p = 2\cos(p)$ and $s = \pm 1$ as before. To determine the transverse wavenumber, the boundary conditions near the N sites are considered. Again, substituting the general form of the wavefunctions into (26), it is found that:

$$\exp(2ip(N+1)) = 1 \qquad \Rightarrow \qquad p = \frac{r}{N+1}\pi, \quad r = 1, 2, 3, \ldots, N. \tag{28}$$

The energy dispersion and density of states for armchair nanoribbons are plotted in figure 4 for various ribbon widths, with the density of states defined as:

$$g(E) = -\frac{1}{\pi}\,\mathrm{Im}\int_{1st\,BZ} \frac{1}{E - E(\mathbf{k}) + i\mu} d\mathbf{k}, \tag{29}$$

where the integral is taken over the first Brillouin Zone and μ is an infinitesimally small number.

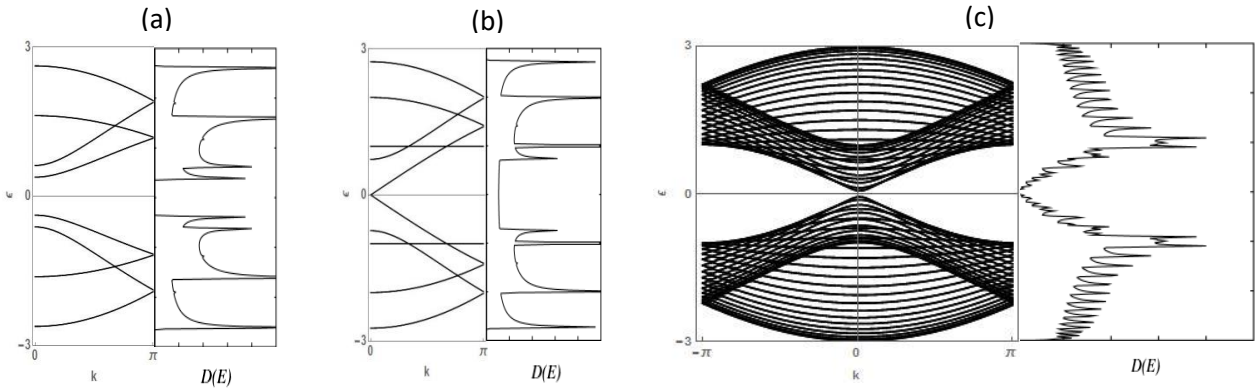

Figure 4 The energy band structures and density of states plots of zigzag nanoribbons of ribbon widths (a) $N = 4$, (b) $N = 5$ and (c) $N = 30$. In these plots, μ is taken to be 0.01 as smaller magnitudes call for longer computational times with negligible improvement on the results. Plotted in Wolfram Mathematica [8].

From the energy dispersion in figure 4, it can be seen that for $N=5$, that $E_s=0$ when $k=0$ and therefore there is no energy gap, i.e. the nanoribbon is metallic. This property is in fact true whenever $N=3n-1$ for n integer. From equation (27), in general $E_s=s(1+2\cos(p))$ for $k=0$ which gives an energy gap Δ_a between the conduction and valance band. This energy gap is given by:

$$\Delta_a=\begin{cases}0, & N=3m-1,\\ 2t\left[1+\cos\left(\dfrac{3m}{3m+1}\right)\right], & N=3m,\\ 2t\left[1+\cos\left(\dfrac{3m+1}{3m+2}\right)\right], & N=3m+1,\end{cases} \tag{30}$$

where $m=1,2,3,\ldots$. Either by plotting the energy as a function of the nanoribbons width directly or by performing a Taylor expansion, it is possible to show that:

$$\Delta_a\sim\begin{cases}0, & N=3m-1,\\ \dfrac{\pi}{W+\sqrt{3}/2}, & N=3m,\\ \dfrac{\pi}{W}, & N=3m+1,\end{cases} \tag{31}$$

where W is the ribbon width of the nanoribbon in the unit of the lattice constant a. Therefore, for all widths, the energy gap is inversely proportional to the width.

3. Zigzag graphene nanoribbons

As with the Armchair nanoribbons, a simple model is used to investigate the electronic structure, as shown in figure 5.

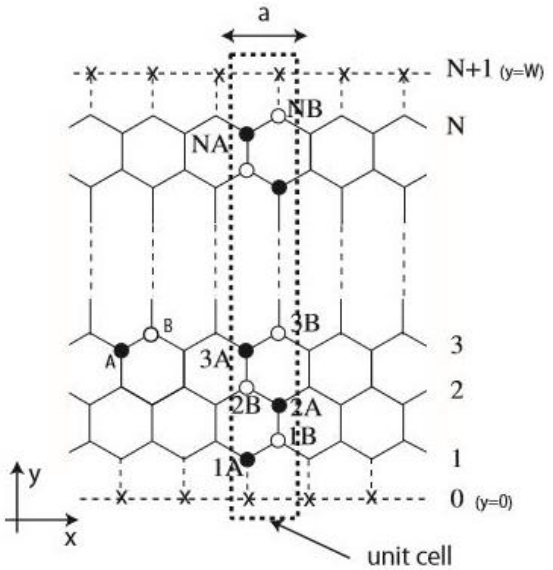

Figure 5. Diagram depicting the model for graphene zigzag nanoribbons, where the "x" signals determination of the graphene sheet by a hydrogen atom which does not contribute to the electron band structure. The dotted box labels the unit cell for this structure. Adapted from [11].

The tight binding Hamiltonian for the zigzag system can be explicitly written as [11]:

$$\begin{aligned} H = &-t\sum_{l}\sum_{m=1}^{N}\left[a_l^{\dagger}(m)b_{l-1}(m)+b_l^{\dagger}(m)a_l(m)\right]+h.c. \\ &-t\sum_{l}\sum_{m=1}^{N-1}a_l^{\dagger}(m+1)b_l(m)+h.c. \end{aligned}, \tag{32}$$

where the creation and annihilation operators are defined as before and the first line in (32) corresponds to longitudinal electron hopping in the *x*-direction with the second line describing transverse hopping in the *y*-direction. Following the same methodology as the armchair system, but now performing a Fourier transform along the *x*-axis:

$$a_l(m)=\frac{1}{\sqrt{L_x}}\sum_k \exp\left(ikx_{l,mA}\right)\alpha_k(m), \quad b_l(m)=\frac{1}{\sqrt{L_x}}\sum_k \exp\left(ikx_{l,mB}\right)\beta_k(m), \tag{33}$$

where L_x is the number of unit cells in the system. Substituting (33) into the Hamiltonian (32) and introducing the one-particle state in the Schrödinger equation give the equations of motion:

$$\left.\begin{aligned} E\psi_{m,A} &= -\psi_{m-1,B}-g_k\psi_{m,B}, \\ E\psi_{m,B} &= -\psi_{m+1,A}-g_k\psi_{m,A}, \end{aligned}\right\}\ m=0,1,2,3,\ldots,N+1. \\ E\psi_{1,A} = -g_k\psi_{1,b}, \\ E\psi_{N,B} = -g_k\psi_{N,A} \tag{34}$$

where $g_k = 2\cos\left(k/2\right)$, and the equations of motion have been modified at the edges, assuming the boundary conditions $\psi_{0,B}=\psi_{N+1,A}=0$. Again, assuming general forms of the wavefunctions yields a matrix equation:

$$\begin{vmatrix} E\left(e^{ipm}-z^2e^{-ipm}\right) & \left(g_k+e^{-ip}\right)e^{ipm}-\left(g_k+e^{ip}\right)e^{-ipm} \\ \left(g_k+e^{ip}\right)e^{ipm}-\left(g_k+e^{-ip}\right)z^2e^{-ipm} & E\left(e^{ipm}-e^{-ipm}\right) \end{vmatrix}=0, \tag{35}$$

where $z=\exp\left(ip(N+1)\right)$. Before directly solving, it should be noticed that some values of the transverse wavenumber $p=0,\pm\pi$ should be excluded as non-physical, as for these values, equation (35) is equal to zero. By solving, it is found that (35) has the following form:

$$\chi e^{2ipm}+\nu e^{2ipm}+\sigma=0, \tag{36}$$

where χ,ν and σ all functions of E, g_k and z. Therefore, χ,ν and σ should all equal zero, from which the energy dispersion is found:

$$E_s = s\sqrt{1+g_k^2+2g_k\cos(p)}\ , \tag{37}$$

with all terms being as previously defined. However, the equation is not readily available as there are not yet any behaviours set onto the transverse wavenumber. By using the fact that $\sigma=0$ and using (37) to eliminate E, it is obtained:

$$F(p,N) \equiv \sin(pN) + g_k \sin(p(N+1)) = 0. \tag{38}$$

This dependence of the transverse wavenumber on the longitudinal wavenumber k causes a complication which is not present in the armchair system and therefore requires further analysis. These properties of the transverse wavenumber are also derivable from the massless Dirac equation [12]. As the sine function is a periodic and odd function, it follows that (38) is also periodic and odd, such that only solutions in the range $0 < p < \pi$ are needed. By plotting $F(p, N = 4)$ for a range of g_k, as shown in figure 6, it can be seen that under a critical value g_k^c, there are $N-1$ solutions for p and N solutions when over this critical value.

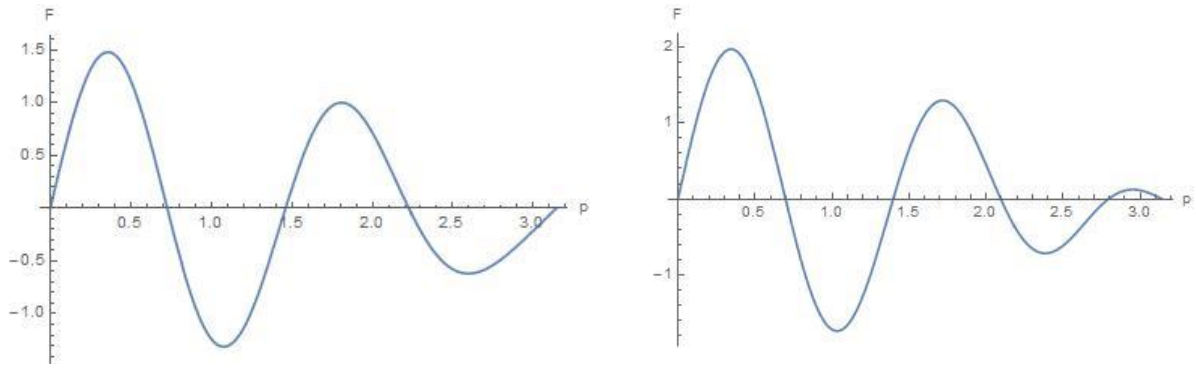

Figure 6. Plots of equation (38) as a function of the transverse wavenumber for values (a) $g_k = 0.5$ and (b) $g_k = 1$. As discussed in the text, the solutions for p at 0 and π are considered unphysical so are excluded, giving three solutions in (a) and four solutions in (b).

As shown in figures 6(a) and 6(b) with $g_k = 0.5$ and $g_k = 1$ respectively, that the critical value must be between the two values and can be found by producing plots with varying g_k until the transition is found. However, it can be found analytically that this critical value can be found from:

$$\frac{\partial}{\partial p} F \bigg|_{p=\pi} = 0 \qquad \Rightarrow \qquad g_k^c = \pm \frac{1}{1 + 1/N}, \tag{39}$$

i.e. the critical value depends on the ribbon width. It should be noted that for $|g_k| < g_k^c$, there is a solution missing when compared to $|g_k| \geq g_k^c$, which can be found by analytical continuation [12] and allowing the wavenumber to become complex. Hence, it can be written as:

$$p \to \begin{cases} \pi \pm i\eta \equiv p_\pi & k_c^L < |k| < \pi, \\ 0 \pm i\eta \equiv p_0 & \pi < |k| < k_c^R, \end{cases} \tag{40}$$

where k_c^L and k_c^R are two solutions of the critical value of the longitudinal wavenumber k_c which can be found from (39) with $k_c^L < k_c^R$. Using the new expressions (40), the energy spectrum and F are now modified:

$$E_s = \begin{cases} s\sqrt{1+g_k^2-2g_k\cosh\eta}, & p=p_\pi, \\ s\sqrt{1+g_k^2+2g_k\cosh\eta}, & p=p_0, \end{cases}$$

$$G(\eta,N)\equiv \sinh(\eta N)-g_k\sinh(\eta(N+1))=0. \tag{41}$$

Plotting $G(\eta,N=4)$, reveals that G has a non-zero solution for $0<g_k<\left|g_k^c\right|$ as shown in figure 7 for $g_k=0.45$.

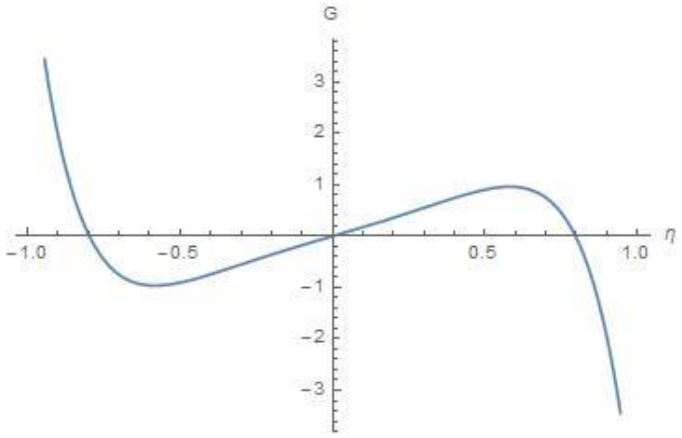

Figure 6. Plot of $G(\eta,N=4)$ as a function of the imaginary component of the transverse wavenumber for value $g_k=0.45$. It can be seen that a solution exists for this value, however as g_k increases, the solution can be seen to vanish. Technically there is a solution at $\eta=0$, however this is considered to be unphysical as discussed in the text.

Numerically finding these solutions for the wavenumber allows the energy band structure to be found for the zigzag nanoribbons, which are plotted in figure 7 for $N=4,5,30$.

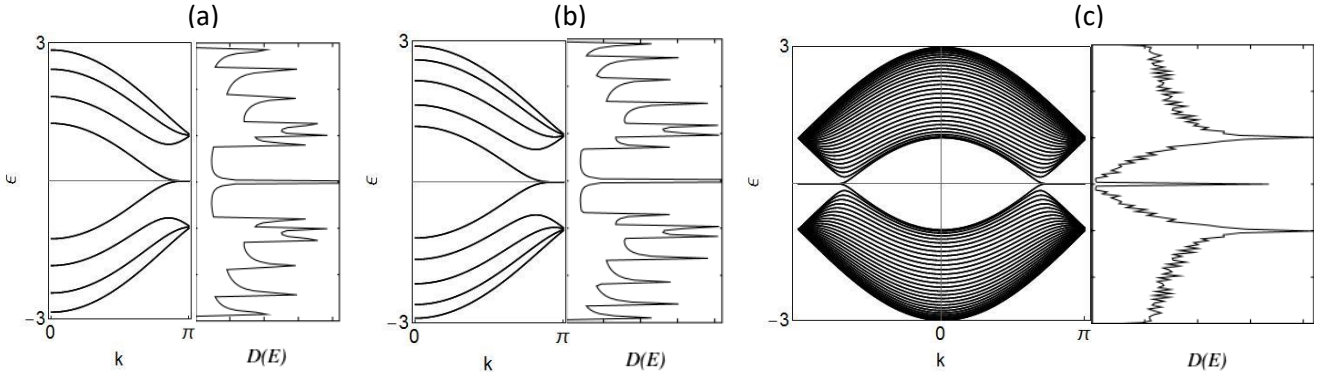

Figure 7. The energy band structures and density of states plots of zigzag nanoribbons of ribbon widths (a) $N=4$, (b) $N=5$ and (c) $N=30$.

It can be seen that partially flat bands exist in this geometry for zero energy, and that the zigzag ribbon is always conducting, i.e. there is no intrinsic band gap.

4. Armchair and zigzag graphene nanoribbons in a magnetic field

After the discovery of graphene, many experiments were undertaken to fully comprehend its electronic properties. One of which is the existence of the Quantum Hall Effect (QHE) where

under a large magnetic field, the resistance across the width of the sample becomes quantised, and electrons are allowed to travel without resistance along the edges of the sample [13]. The possibility of creating a zero resistance current is important to a large range of applications, especially when the superconducting material is relatively easy to produce, with such a lot of research and interest in this area that is present in the literature. In order to fully understand the mechanisms that allow this behaviour, the motion of a two-dimensional gas of electrons, which exists in graphene, must be understood in a magnetic field. As seen previously, the electrons in graphene behave as relativistic massless fermions and are such described by the Dirac equation. However, under a magnetic field the canonical kinetic momentum is replaced by the gauge invariant version in the so-called Peierls substitution:

$$\mathbf{p} \to \mathbf{\Pi} = \mathbf{p} + e\mathbf{A}(\mathbf{r}), \tag{42}$$

where $\mathbf{A}(\mathbf{r})$ is the usual vector potential which generates the field $\mathbf{B} = \nabla \times \mathbf{A}(\mathbf{r})$ which is perpendicular to the plane of the lattice. As this substitution is made for electrons on a lattice, it is only valid as long as the lattice spacing distance a is less than the magnetic length, which is defined as:

$$l_B = \sqrt{\frac{\hbar}{eB}}. \tag{43}$$

The condition of $a < l_B$ in graphene may be achieved in modern high-field laboratories with $B \sim 45\mathrm{T}$. Thus the field free Hamiltonian is transformed as $H(\mathbf{p}) \to H(\mathbf{\Pi})$ which is no longer translation invariant due to the position dependence of the vector potential, while the canonical momentum $\mathbf{p} = \hbar\mathbf{q}$ is no longer conserved. The Dirac Hamiltonian to lowest order in q then becomes:

$$H_B^{\xi} = \xi\hbar v_F\left(q_x\sigma^x + q_y\sigma^y\right) \to \xi v_F\left(\Pi_x\sigma^x + \Pi_y\sigma^y\right), \tag{44}$$

where σ are the usual Pauli matrices. In general, the energy of the Hamiltonian (44) is separated into two branches due to the Zeeman effects, however is found that the characteristic behaviour of the energy band structure develops from the orbital degrees of freedom and such only spinless fermions are considered [14]. Quantisation of this Hamiltonian is achieved by use of the commutator relation:

$$\left[A_1, f(A_2)\right] = \frac{df}{dA_2}\left[A_1, A_2\right], \tag{45}$$

where $A_{1,2}$ are arbitrary operators. By (45), the commutation of the gauge invariant momentum can be found:

$$\left[\Pi_x, \Pi_y\right] = -ie\hbar\left(\frac{\partial A_y}{\partial x} - \frac{\partial A_x}{\partial y}\right) = -i\frac{\hbar^2}{l_B^2}, \tag{46}$$

where the Landau gauge has been assumed, i.e. $\mathbf{A}=(0,Bx,0)$. It becomes highly convenient to express these momenta operators in terms of the quantum harmonic ladder operators, which converts the Hamiltonian into a more useful form:

$$\hat{a}=\frac{l_B}{\sqrt{2}\hbar}\left(\Pi_x-i\Pi_y\right), \qquad \hat{a}^\dagger=\frac{l_B}{\sqrt{2}\hbar}\left(\Pi_x+i\Pi_y\right), \tag{47}$$

$$H_B^\xi=\xi\hbar\omega'\begin{pmatrix}0 & \hat{a}\\ \hat{a}^\dagger & 0\end{pmatrix}, \tag{48}$$

where the where the characteristic frequency is $\omega'=\sqrt{2}v_F/l_B$, which plays the role of the relativistic cyclotron frequency. The energy eigenvalues for this system can be found by considering a two-component spinor $\psi_n=\begin{pmatrix}u_n & v_n\end{pmatrix}^\dagger$ and combining with (48) to produce a system of equations which can be solved to find:

$$\varepsilon_n=\lambda\frac{\hbar v_F}{l_B}\sqrt{2n}=\lambda v_F\sqrt{2\hbar eBn}\,, \tag{49}$$

where $\lambda=\pm1$ correspond to positive and negative energy solutions and $n\geq0$. These energy levels are named the relativistic Landau Levels (LL) and are plotted in figure 8.

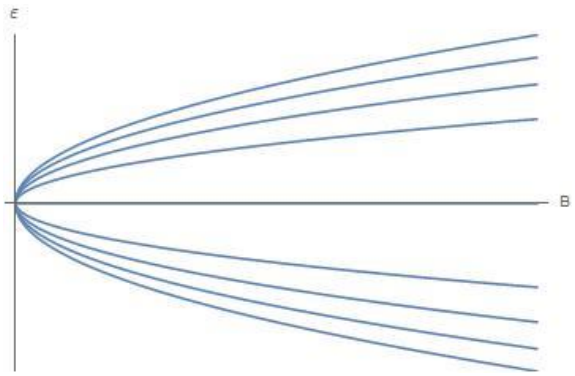

Figure 8. Plot showing the general behaviour of the energy levels of electrons while present in a magnetic field perpendicular to the plane of the lattice. Note that at the zero field limit, the energy levels become two-fold degenerate. The energy of the LLs increase with increasing *n*. Values of the energy with *n*=1,2,3,4 are shown in the plot.

While the Landau levels give the description of the energy levels of electrons in a general graphene sheet, it gives no information of the behaviour of the edge states or the effects of making the system finite. To this end, the tight-binding model is again used with a simple Hamiltonian:

$$H=\sum_{\langle i,j\rangle}t_{ij}c_i^\dagger c_j, \tag{50}$$

where as usual, the operator $c_i^\dagger\left(c_i\right)$ creates (destroys) an electron at site *i*. This Hamiltonian is different to the one used previously, as now the transfer integral t_{ij} is site-

dependant. This is done such that the magnetic field is included in the Hamiltonian by the Peierls phase, which is defined as:

$$t_{ij} \to t_{ij} e^{2i\pi\phi_{i,j}}, \tag{51}$$

where $\phi_{i,j}$ is defined as the line integral of the vector potential from site i to j:

$$\phi_{i,j} = \frac{e}{ch}\int_{i}^{j} d\mathbf{l}\cdot\mathbf{A}, \tag{52}$$

with the magnetic flux through arbitrary area $\mathbf{S}$ in units of the magnetic flux quantum $\phi_0 = ch/e$:

$$\sum_{around\ \mathbf{S}} \phi_{i,j} = \frac{e}{ch}\oint d\mathbf{l}\cdot\mathbf{A} = \frac{1}{\phi_0}\int d\mathbf{S}\cdot\mathbf{B}, \tag{53}$$

where a Landau gauge is assumed as before. In order to apply the Hamiltonian (50) to the graphene lattice, it is highly convenient to transform the hexagonal lattice structure into a brick-like structure which conserves the lattice topology [15] as shown in figure 9.

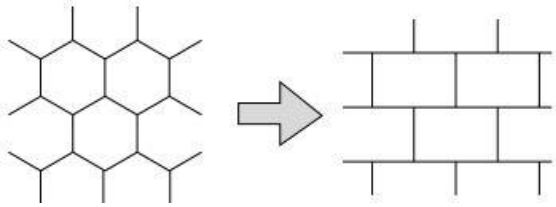

Figure 9. A figurative drawing of the transformation from the hexagonal lattice to the brick-like lattice which conserves the lattice topology and simplifies the equations [11].

For each lattice, we define the translational invariant direction of the ribbons as the $\hat{\mathbf{y}}$ direction, with the $\hat{\mathbf{x}}$ direction perpendicular. Using equation (52), it is found that the Peierls phase for both the zigzag and armchair lattices in the Laudau gauge is given by $\phi_{mB,nA} = m\phi\delta_{nm}/2$ where ϕ is the magnetic flux through the lattice in units of the quantum flux. A diagram showing the Peierls phase across the brick zigzag and armchair lattices is shown in figure 10.

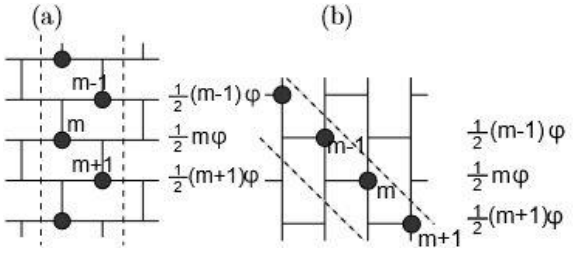

Figure 10. The brick-like versions of the (a) zigzag and (b) armchair lattices where the Peierls phase is given at the mth site in the Landau gauge [11].

In a similar fashion to previous considerations, to compute the equations of motion of the zigzag ribbons, a Fourier transformed creation operator for the electrons in the system in the translational invariant direction is introduced:

$$c_\alpha(i) = \frac{1}{\sqrt{L}} \sum_k e^{ikr_\alpha} \gamma_k(i), \tag{54}$$

where the position of the unit cell α is given by r_α. By defining a one-particle state in terms of the creation operator and combining with the Hamiltonian and Schrödinger equation, eigenvalue equations for the energy at various sites are obtained:

$$\begin{aligned}
\varepsilon\Psi_{mB} &= \Psi_{(m+1)A} + e^{2i\pi m\phi/2}\Psi_{mA} + e^{-2i\pi m\phi/2}\Psi_{mB}, \\
\varepsilon\Psi_{mA} &= \Psi_{(m-1)B} + e^{2i\pi m\phi/2}\Psi_{mB} + e^{-2i\pi m\phi/2}\Psi_{mB}, \\
\varepsilon\Psi_{(m+1)A} &= \Psi_{mB} + e^{2i\pi m\phi/2}\Psi_{(m+1)B} + e^{-2i\pi m\phi/2}\Psi_{(m+1)B}.
\end{aligned} \tag{55}$$

Through these equations, it is possible to eliminate the A-sublattice sites to find a difference equation for the B-sublattice:

$$\lambda\Psi_m(k_y) = a_m\Psi_{m+1}(k_y) + b_m\Psi_m(k_y) + a_{m-1}\Psi_{m-1}(k_y), \tag{56}$$

where $\lambda = \varepsilon^2 - 3$, $a_m(k_y) = 2\cos(k_y/2 + m\pi\phi)$, $b_m(k_y) = 2\cos(k_y + 2m\pi\phi)$ and $\Psi_{mB} = \Psi_m$. This simplifies the problem as it has been reduced to a one-dimensional tight-binding model, where so far no boundary conditions have been assumed, i.e. this can be applied to both graphene sheets and ribbons with the appropriate boundary conditions. The factor of $m\pi\phi$ in a_m will be replaced by $((N-1)/2 - m + 1)\pi\phi$ as this keeps the energy dispersion symmetric about $k = 0$ for some arbitrary magnetic flux. Similarly, a difference equation can be obtained for the armchair ribbon:

$$\lambda\Psi_m(k_y) = \Psi_{m+2}(k_y) + a_m\Psi_{m+1}(k_y) + a_m\Psi_{m-1}(k_y) + \Psi_{m-2}(k_y), \tag{57}$$

where $\lambda = \varepsilon^2 - 3$ and $a_m(k_y) = 2\cos(k_y/2 + (m - 1/2)\pi\phi)e^{-i\pi\phi/2}$. Again, a_m is shifted such to keep the energy band symmetric, $a_m(k_y) = 2\cos(k_y/2 + ((N-1)/2 - 2m + 3)\pi\phi)e^{-i\pi\phi}$. The two equations (56) and (57) are known as the Harper equations in the literature [16,17]. By considering the zero-field case in equations (56) and (57), the energy dispersions for the zigzag and armchair ribbons can be found as previous which is encouraging that assumptions made are valid. However, in order to yield the energy dispersion for non-zero magnetic field it is possible to express the eigenvalue problem as a system of q equations for a rational magnetic field flux $\phi = p/q$. Forming a matrix equation and finding the determinant of the $q \times q$ secular matrix allows the energy dispersion to be plotted, as shown in figure 11. It is interesting to notice that in the limit of low magnetic field, the Landau levels can clearly be seen, however with increasing magnetic field, the levels form subbands due to Harper broadening. The degeneracy at zero energy is also conserved for any arbitrary flux, which confirms the existence of the *K*-point degeneracy.

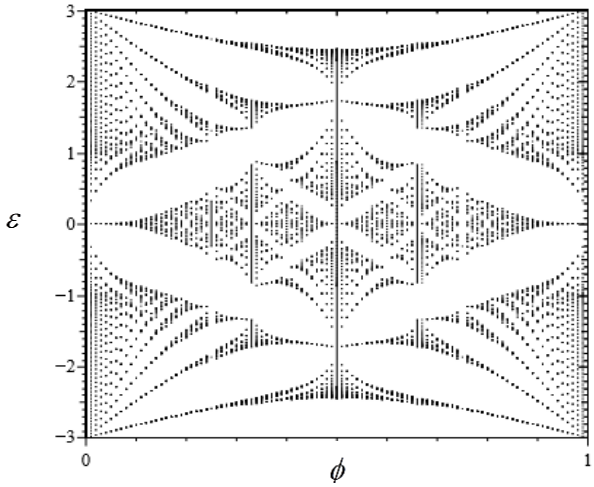

Figure 11. The energy dispersion as a function of the rational magnetic flux, where the energy is plotted along the vertical axis and the magnetic flux along the horizontal. This band structure has a recursive property and resembles the structure of the so-called Hofstadter Butterfly [18].

As mentioned, the energy dispersions of the armchair and zigzag nanoribbons can be obtained by imposing boundary conditions on the Harper equations. For both nanoribbons, the boundary condition at the edges is $\Psi_{N+1} = \Psi_0 = 0$, however the edge sites need more careful consideration. In the zigzag Harper equation, the fact that the $0A(B)$ and $(N+1)A(B)$ sites do not exist was not included, requiring that at the $m = 1, N$ sites equation (56) must be modified:

$$\lambda\Psi_m(k_y) = a_m\Psi_{m+1}(k_y) + (b_m - 1)\Psi_m(k_y) = a_{m-1}\Psi_{m-1}(k_y), \tag{58}$$

with a similar substitution in equation (57), due to the $0A$ and $(N+1)A$ not existing for the armchair ribbons. The energy dispersion for zigzag nanoribbons are shown in figures 12(a)-(d), for $\phi = 0, 1/500, 1/100, 1/4$ respectively, all with $N = 50$.

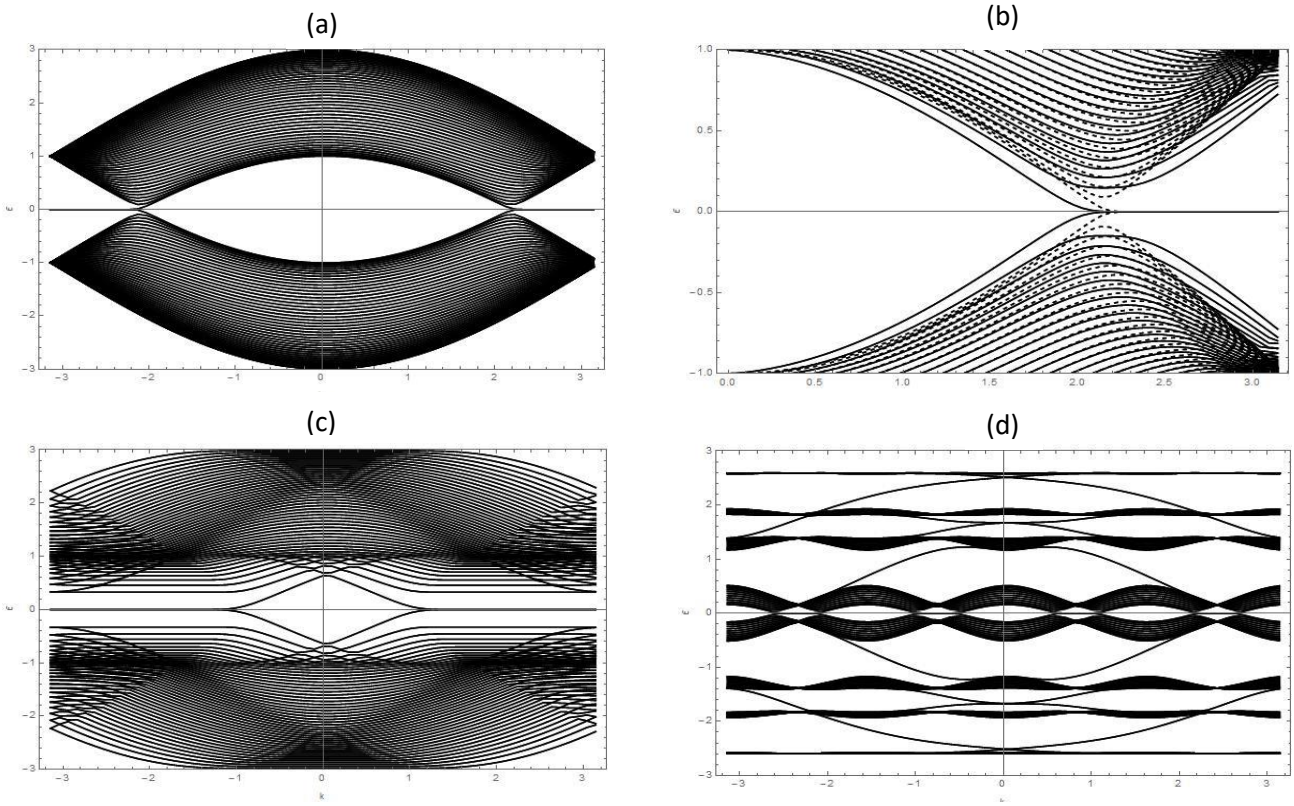

Figure 12. The energy dispersions of zigzag nanoribbons at magnetic flux values of (a) $\phi = 0$, (b) $\phi = 1/500$, (c) $\phi = 1/100$ and (d) $\phi = 1/4$, all with a width of $N = 50$. For comparison, the energy dispersion for zero field is plotted as a dashed line in (b).

The presence of the edge states in the zigzag ribbons can be seen in the zero-field energy dispersion by the existence of partial flat bands at $\varepsilon = 0$, which does not appear in the infinite graphene sheet [11]. For small values of the magnetic flux, i.e. for $q \geq N$, the energy band structure barely changes as the edges of the ribbons interrupt the electron's cyclotron motion, and the Landau levels are also not perfectly formed. For larger ribbons with $q \leq N$, the cyclotron motion is sufficiently small such that the edges do not affect the electrons, allowing the Landau levels to become more developed. In the more extreme case of $q << N$, i.e. $\phi = 1/4$, it is seen that the such labelled "2 x 4"-Landau subbands form. However, there are also additional dispersions seen between the subbands which do not appear in the graphene sheet and are therefore localised states along the edges caused by the cyclotron motion and not topological effects [19]. It is worth noting also that the partially flat bands are also present for $\varepsilon = 0$ in the large magnetic field case.

The energy dispersion for the armchair nanoribbons are given in figures 13(a)-(d) for the same respective magnetic fluxes as in the zigzag case with the same ribbon width.

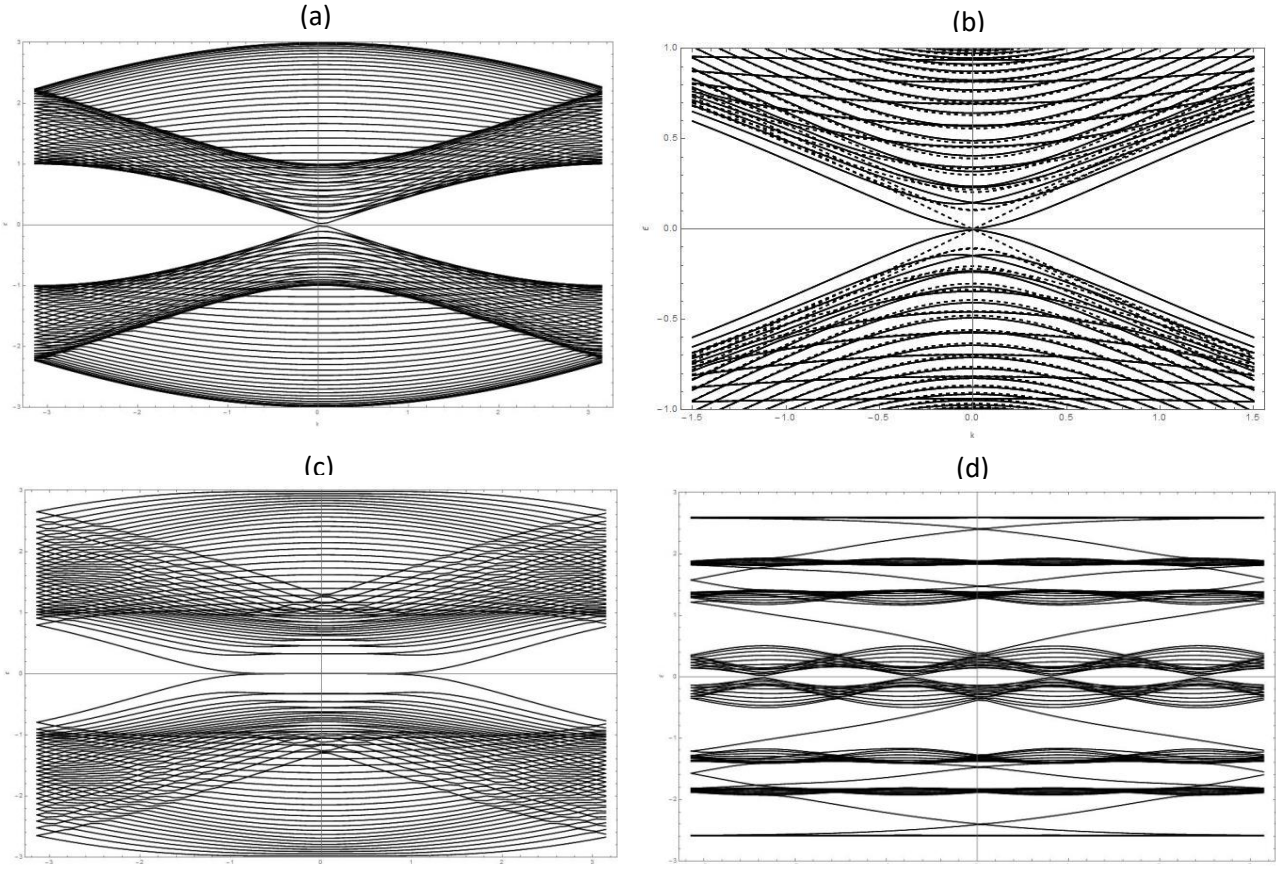

Figure 13. The energy dispersions of armchair nanoribbons at magnetic flux values of (a) $\phi = 0$, (b) $\phi = 1/500$, (c) $\phi = 1/100$ and (d) $\phi = 1/4$, all with a width of $N = 50$. For comparison, the energy dispersion for zero field is plotted as a dashed line in (b).

In the zero field case, the armchair ribbon does not have partially flat bands at $\varepsilon = 0$, indicating the absence of edge states for this geometry. For small magnetic fields $q \geq N$, the Landau levels are not yet perfectly formed, with the energy bands hardly changing from the zero field case. With increasing magnetic field $q \leq N$, the Landau levels begin to

become clearly seen as the ribbon width is now large compared to the cyclotron radius. Finally, for large magnetic fields $q << N$, the 2 x 4-Landau subbands are formed with additional dispersion between the subbands. However, even with these additional dispersions, there are still no partially flat bands present in the armchair ribbons even in a magnetic field.

It is possible to investigate the edge state in the zigzag ribbon further by solving the Harper equation (56) in a transfer matrix form [20]:

$$\begin{pmatrix} \Psi_{m+1} \\ \Psi_m \end{pmatrix} = \begin{pmatrix} \frac{1}{a_m}\left(\lambda - \bar{b}_m\right) & \frac{a_m - 1}{a_m} \\ 1 & 0 \end{pmatrix} \begin{pmatrix} \Psi_m \\ \Psi_{m=1} \end{pmatrix}, \tag{59}$$

where $\bar{b}_m = b_m - 1$ near the edges and takes the value b_m everywhere else. Assuming open boundary conditions for the wavefuctions, i.e. $\begin{pmatrix} \Psi_1 & \Psi_0 \end{pmatrix}^T = \begin{pmatrix} 1 & 0 \end{pmatrix}^T$ and imposing that $\varepsilon = 0$, it can be found that for zero magnetic field:

$$\Psi_n = \left(-2\cos\left(\frac{k}{2}\right)\right)^{n-1} = D_k^{n-1}. \tag{60}$$

For this wavefunction to converge, it is required that $|D_k| \le 1$ which defines the region $2\pi/3 \le k \le \pi$, which is where the partially flat bands are located. By considering the charge density at $k = \pi$, it is found that it is zero everywhere except the $n = 1$ site, which corresponds to the edge, i.e. the charge is exactly localised at the edge of the zigzag ribbon. As the wavenumber moves away from this value, the charge density penetrates further into the ribbon. A diagrammatic picture of this phenomenon is shown in figure 14 for different values of the wavenumber.

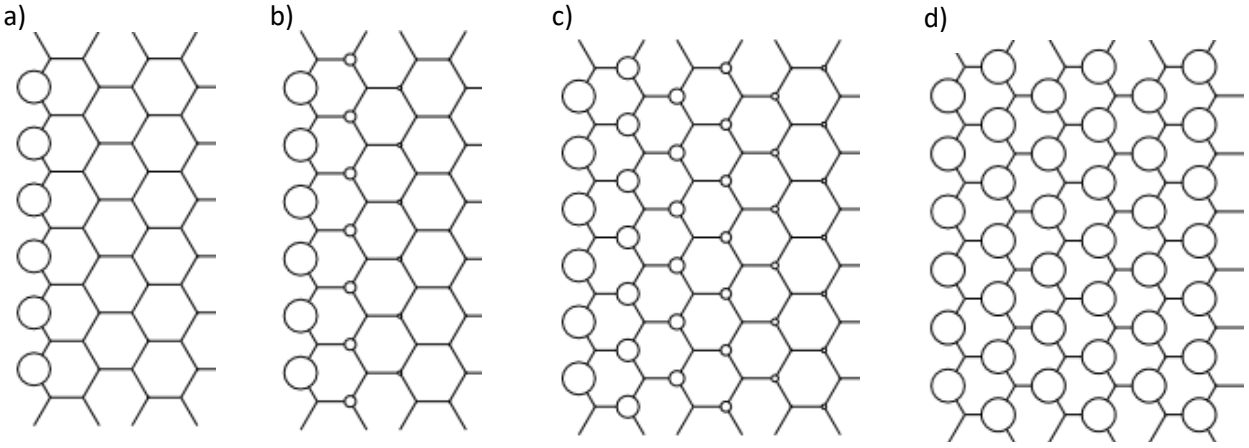

Figure 14. Charge density of the edge state in the zigzag ribbon with wavenumbers (a) $k = \pi$, (b) $k = 8\pi/9$, (c) $k = 7\pi/9$, (d) $k = 2\pi/3$, where the magnitude of the charge density of represented by the size of the circles at each site. Adapted from [11].

Now taking the case of a finite magnetic field with the condition $\varepsilon = 0$, the wavefunction of the *n*-th zigzag line can be found as:

$$\Psi_n = \Pi_{i=1}^{n} D_k(i), \tag{61}$$

$$D_k(i) = \begin{cases} -2\cos\left(\dfrac{k}{2} - \dfrac{N-2i+1}{2}\pi\phi\right) & (i \le 2) \\ 1 & (i = 1) \end{cases}. \tag{62}$$

Using the fact that there exists a periodic relation $D_k(i) = D_k(i+q)$, where q is defined in terms of the magnetic flux, allows equation (61) to be rewritten as:

$$\Psi_{nq} = \left(\Pi_{i=1}^{q} D_k(i)\right)^{n-1} = (\Delta_k)^{n-1}, \tag{63}$$

i.e. the edge states become modified in the presence of a magnetic field. The region of the flat bands are now defined by the condition that $\Delta_k \le 1$, which is required for the wavefunction to converge. It is a particularly interesting property that as Δ_k has q factors of D_k, each of which can separately equal zero, then Δ_k has q internal degrees of freedom. For example, in the case of $\phi = 1/4$, there are four zeros of Δ_k given by the wavenumbers $k = \pm 3\pi/4, \pm\pi/4$. The charge density distributions corresponding to these wavenumbers are shown in figures 15(a)-(d).

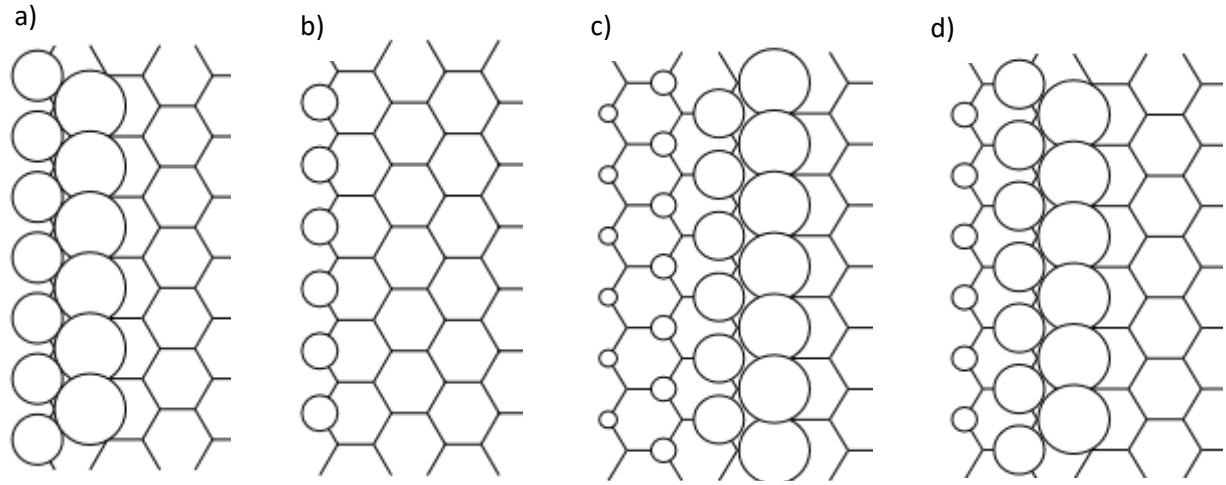

Figure 15. Charge density of the edge state in the zigzag ribbon with wavenumbers (a) $k = -3\pi/4$, (b) $k = -\pi/4$, (c) $k = \pi/4$, (d) $k = 3\pi/4$, where the magnitude of the charge density of represented by the size of the circles at each site. Adapted from [11].

It can be seen that the charge density does not penetrate into the ribbon further than the $(4+1)$-th zigzag line with the four internal degrees of freedom producing four kinds of localised modes. This form of electron confinement possible due to the edge states gives promise to applications in areas such as magnetic quantum dots and magnetic spin currnets [21].

Conclusion

In this report, the tight binding model of electrons in graphene has been presented in the cases for both infinite sheets and finite nanoribbons, with and without external magnetic fields. This model is very successful in deriving the energy dispersions and density of states

for the graphene sheet, and both armchair and zigzag nanoribbons geometries. It is also possible to derive many physical observables using this theory, for example the magnetic susceptibility and quantum hall effect, and while these topics have not been discussed here, there exists many papers covering these areas in the literature. The armchair and zigzag nanoribbons have many interesting intrinsic properties, however the most interesting are the existence of a partially flat band edge state in zigzag nanoribbons, which many have applications in superconductivity, and the width-dependant conducting properties of the armchair nanoribbons. The edge state has been investigated with and without a magnetic field, and it has been shown how the magnetic field affects the edge state, evolving into an electron confinement system, which may have applications in quantum dots. While only a constant magnetic field perpendicular to the graphene plane has been considered, studies exist which explore both inhomogeneous fields [22] and irrational fields [23] which give further electronic properties. While it has not been investigated in this report, the quantum Hall effect, which describes a discretised resistance of the electrons in graphene, is very important in the field of graphene as it has huge superconductivity potential and the ability to produce large magnetic fields, which would have application in medical devices, geology, and nuclear reactors.

The tight binding model used throughout this paper is successful in deriving the electronic principles of graphene in various geometries, simplifying the formula compared to other methods. This work could be taken further by considering next nearest neighbour hopping, electron-electron interactions or electron-phonon interactions, to further develop the theory. A wave mechanics approached has been utilised when analytically deriving the energy spectrums of the zigzag and armchair nanoribbons in the absence of a magnetic field, however this become much more complex when considering a magnetic field, so numerically solving the Hamiltonian from which the Harper equations come from became necessary. This numerical method appears to be popular in the literature, with the dispersions produced in this paper practically identical to results found by other authors [11,24], with not much computational power or time required.

References

[1] McCann, E. (2012). Electronic properties of monolayer and bilayer graphene. arXiv:1205.4849v1 [cond-mat.mes-hall].

[2] Han, W. Kawakami, R. K. Gmitra, M. Fabian, J. (2014). Graphene spintronics. Nature Nanotechnology 9, 794-807.

[3] Schwarz, S. (2011). Properties of Graphene in an External Magnetic Field. Bachelor Thesis. Albert Einstein Center for Fundamental Physics.

[4] MacDonald, A. H. Barlas, Y. Yang, K. (2011). Quantum Hall Effects in Graphene-Based Two-Dimensional Electron Systems. arXiv:1110.1069v1 [cond-mat.mes-hall].

[5] Arikawa, M. Hatsugai, Y. Aoki, H. (2013). Edge states in graphene in magnetic fields – a speciality of the edge mode embedded in the n=0 Landau band. arXiv:0805.3240v1 cond-mat.mes-hall].

[6] Kundu, R. (2009). Tight binding parameters for graphene. arXiv:0907.4264v1 cond-mat.mes-hall].

[7] Neto, A. H. C. et al. (2009) The electronic properties of graphene. RevModPhys.81.109.

[8] Wolfram Research, Inc., Mathematica, Version 10.0.2.0, Champaign, IL (2014).

[9] Tian, J. et al. (2011). Direct imaging of graphene edges: atomic structure and electronic scattering. Nano Lett. 11, 3663-3668.

[10] Sugawara, K. Sato, T. Souma, S. Takahashi, T. Suematsu, H. (2006) Phys. Rev. B 73 045124

[11] Wakabayashi, K. Sasaki, K. Nakanishi, T. Enoki, T. (2010). Electronic states of graphene nanoribbons and analytical solutions. Sci. Technol. Adv. Mater. 11, 054504

[12] Wakabayashi, K. (2000). Low-energy physical properties of edge states in Nano-graphites. PhD Thesis. University of Tsukuba

[13] He, K. (2015). The Quantum Hall Effect gets More Practical. APS Physics 8,41.

[14] Goerbig, M. O. (2011). Electronic properties of graphene in a Strong Magnetic Field. RevModPhys.83.1193.

[15] Hou, J. M. Chen, W. (2014). Hidden symmetry and protection of Dirac points on the honeycomb lattice. Sci. Rep. 5, 17571.

[16] Bernevig, B, A. Hughes, T, L. Zhang, S, C. (2006). Band Collapse and the Quantum Hall Effect in Graphene. Internaltional Jornal of Modern Physics B Vol. 20, No. 22 3257-3278.

[17] Park, K. Rhim, J, W. (2012). Self-similar occurrence of massless Dirac particles in graphene under magnetic field. Phys. Rev. B, 86.235411.

[18] Rammal, R. (1985). Landau level spectrum of Bloch electrons in a honeycomb lattice. J. Phys. France 46, 1345-1354.

[19] MacDonald, A. H. Streda, P. (1984). Quantized Hall effect and edge currents. Phys. Rev. B 29, 1616.

[20] Rüdinger, A. Piéchon, F. (1996). Hofstadter rules and generalized dimensions of the spectrum of Harper's equation. J. Phys. A: Math. Gen. 30 117.

[21] Murguia, G. (2010). Magnetic Edge States in Graphene. Proceedings of XII Mexican Workshop on Particles and Fields, Mazatlan, Sinaloa, Mexico.

[22] Masir, M. R. Vasilopoulous, P. Peeters, F. M. (2011). Graphene in inhomogenous magnetic fields: bound quasi-bound and scattering states. J. Phys.: Condens. Matter 23 315301.

[23] Hofstadter, D. R. (1976). Energy levels and wave functions of Bloch electrons in rational and irrational magnetic fields. PhysRevB.14.2239.

[24] Enoki, T. Ando, T. (2013). Physics and Chemistry of Graphene: Graphene to Nanographene. Pan Stanford Publishing. 546.681.